RESEARCH ARTICLE SUMMARY

MOLECULAR BIOLOGY

Coactivator condensation at super-enhancers links phase separation and gene control

Benjamin R. Sabari*, Alessandra Dall'Agnese*, Ann Boija, Isaac A. Klein, Eliot L. Coffey, Krishna Shrinivas, Brian J. Abraham, Nancy M. Hannett, Alicia V. Zamudio, John C. Manteiga, Charles H. Li, Yang E. Guo, Daniel S. Day, Jurian Schuijers, Eliza Vasile, Sohail Malik, Denes Hnisz, Tong Ihn Lee, Ibrahim I. Cisse, Robert G. Roeder, Phillip A. Sharp, Arup K. Chakraborty, Richard A. Young†

INTRODUCTION: Mammalian genes that play prominent roles in healthy and diseased cellular states are often controlled by special DNA elements called super-enhancers (SEs). SEs are clusters of enhancers that are occupied by an unusually high density of interacting factors and drive higher levels of transcription than most typical enhancers. This high-density assembly at SEs has been shown to exhibit sharp transitions of formation and dissolution, forming in a single nucleation event and collapsing when chromatin factors or nucleation sites are deleted. These features led us to postulate that SEs are phase-separated multimolecular assemblies, also known as biomolecular condensates. Phase-separated condensates, such as the nucleolus and other membraneless cellular bodies, provide a means to compartmentalize and concentrate biochemical reactions within cells.

RATIONALE: SEs are formed by the binding of master transcription factors (TFs) at each component enhancer, and these recruit unusually high densities of coactivators, including Mediator and BRD4. Mediator is a large (~1.2 MDa) multisubunit complex that has multiple roles in transcription, including bridging interactions between TFs and RNA polymerase II (RNA Pol II). BRD4 facilitates the release of RNA Pol II molecules from the site of transcription initiation. The presence of MED1, a subunit of Mediator, and BRD4 can be used to define SEs. We reasoned that if transcriptional condensates are formed at SEs, then MED1 and BRD4 should be visualized as discrete bodies at SE elements in cell nuclei. These bodies should exhibit behaviors described for liquid-like condensates. We investigated these possibilities by using murine embryonic stem cells (mESCs), in which SEs were originally described. Because intrinsically disordered regions (IDRs) of proteins have been implicated in condensate formation, we postulated that the large IDRs present in MED1 and BRD4 might be involved.

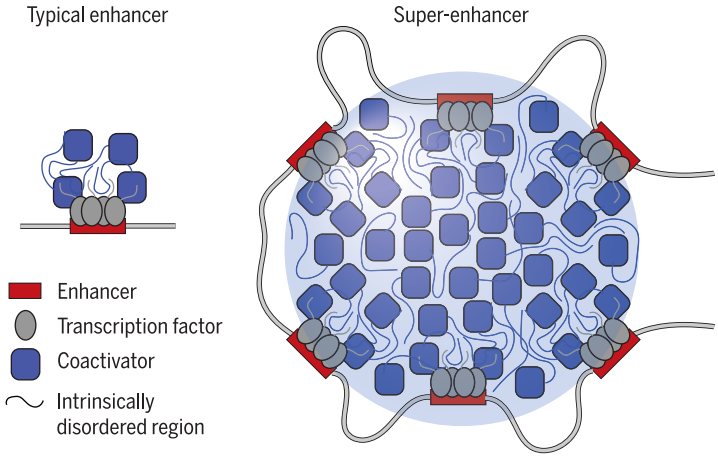

Phase separation of coactivators compartmentalizes and concentrates the transcription apparatus. Enhancers are gene regulatory elements bound by transcription factors that recruit coactivators and the transcription apparatus (not shown) to regulate gene expression. Super-enhancers are clusters of enhancers bound by master transcription factors that concentrate high densities of coactivators and the transcription apparatus to drive robust expression of genes that play prominent roles in cell identity. This is achieved by the phase separation of coactivators, which is driven in part by high-valency and low-affinity interactions of intrinsically disordered regions.

RESULTS: We found that MED1 and BRD4 occupy discrete nuclear bodies that occur at SEs in mESCs. These bodies exhibit properties of other well-studied biomolecular condensates, including rapid recovery of fluorescence after photobleaching and sensitivity to 1,6-hexanediol, which disrupts liquid-like condensates. Disruption of MED1 and BRD4 bodies by 1,6-hexanediol was accompanied by a loss of chromatin-bound MED1 and BRD4 at SEs, as well as a loss of RNA Pol II at SEs and SE-driven genes. The IDRs of both MED1 and BRD4 formed phase-separated liquid droplets in vitro, and these droplets exhibited features characteristic of condensates formed by networks of weak protein-protein interactions. The MED1-IDR droplets were found to concentrate BRD4 and RNA Pol II from transcriptionally competent nuclear extracts, which may reflect their contribution to compartmentalizing and concentrating biochemical reactions associated with transcription at SEs in cells.

ON OUR WEBSITE

Read the full article at http://dx.doi.org/10.1126/science.aar3958

CONCLUSION: Our results show that coactivators form phase-separated condensates at SEs and that SE condensates compartmentalize and concentrate the transcription apparatus at key cell-identity genes. These results have implications for the mechanisms involved in the control of genes in healthy and diseased cell states. We suggest that SE condensates facilitate the compartmentalization and concentration of transcriptional components at specific genes through the phase-separating properties of IDRs in TFs and cofactors. SE condensates may thus ensure robust transcription of genes essential to cell-identity maintenance. These properties may also explain why cancer cells acquire large SEs at driver oncogenes and why SEs that facilitate transcriptional dysregulation in disease can be especially sensitive to transcriptional inhibitors. ■

The list of author affiliations is available in the full article online.
*These authors contributed equally to this work.
†Corresponding author. Email: young@wi.mit.edu
Cite this article as B. R. Sabari *et al.*, *Science* **361**, eaar3958 (2018). DOI: 10.1126/science.aar3958

RESEARCH ARTICLE

MOLECULAR BIOLOGY

Coactivator condensation at super-enhancers links phase separation and gene control

Benjamin R. Sabari[1]*, Alessandra Dall'Agnese[1]*, Ann Boija[1], Isaac A. Klein[1,2], Eliot L. Coffey[1,3], Krishna Shrinivas[4,5], Brian J. Abraham[1], Nancy M. Hannett[1], Alicia V. Zamudio[1,3], John C. Manteiga[1,3], Charles H. Li[1,3], Yang E. Guo[1], Daniel S. Day[1], Jurian Schuijers[1], Eliza Vasile[6], Sohail Malik[7], Denes Hnisz[1], Tong Ihn Lee[1], Ibrahim I. Cisse[8], Robert G. Roeder[7], Phillip A. Sharp[3,6], Arup K. Chakraborty[4,5,8,9,10,11], Richard A. Young[1,3]†

Super-enhancers (SEs) are clusters of enhancers that cooperatively assemble a high density of the transcriptional apparatus to drive robust expression of genes with prominent roles in cell identity. Here we demonstrate that the SE-enriched transcriptional coactivators BRD4 and MED1 form nuclear puncta at SEs that exhibit properties of liquid-like condensates and are disrupted by chemicals that perturb condensates. The intrinsically disordered regions (IDRs) of BRD4 and MED1 can form phase-separated droplets, and MED1-IDR droplets can compartmentalize and concentrate the transcription apparatus from nuclear extracts. These results support the idea that coactivators form phase-separated condensates at SEs that compartmentalize and concentrate the transcription apparatus, suggest a role for coactivator IDRs in this process, and offer insights into mechanisms involved in the control of key cell-identity genes.

Phase separation of fluids is a physicochemical process by which molecules separate into a dense phase and a dilute phase. Phase-separated biomolecular condensates, which include the nucleolus, nuclear speckles, stress granules, and others, provide a mechanism to compartmentalize and concentrate biochemical reactions within cells (*1*–*3*). Biomolecular condensates produced by liquid-liquid phase separation allow rapid movement of components into and within the dense phase and exhibit properties of liquid droplets such as fusion and fission (*4*). Dynamic and cooperative multivalent interactions among molecules, such as those produced by certain intrinsically disordered regions (IDRs) of proteins, have been implicated in liquid-liquid phase separation (*5*–*7*).

Enhancers are gene regulatory elements bound by transcription factors (TFs) and other components of the transcription apparatus that function to regulate expression of cell type–specific genes (*8*–*13*). Super-enhancers (SEs)—clusters of enhancers that are occupied by exceptionally high densities of transcriptional machinery—regulate genes with especially important roles in cell identity (*14*, *15*). DNA interaction data show that enhancer elements in the clusters are in close spatial proximity with each other and the promoters of the genes that they regulate (*16*–*18*), consistent with the notion of a dense assembly of transcriptional machinery at these sites. This high-density assembly at SEs has been shown to exhibit sharp transitions of formation and dissolution, forming as the consequence of a single nucleation event (*19*, *20*) and collapsing when concentrated factors are depleted from chromatin (*21*–*25*) or when nucleation sites are deleted (*26*–*29*). These properties of SEs led to the proposal that the high-density assembly of biomolecules at active SEs is due to phase separation of enriched factors at these genetic elements (*30*). Here we provide experimental evidence that the transcriptional coactivators BRD4 and MED1 (a subunit of the Mediator complex) form condensates at SEs. This establishes a new framework to account for the diverse properties described for these regulatory elements and expands the known biochemical processes regulated by phase separation to include the control of cell-identity genes.

[1]Whitehead Institute for Biomedical Research, 455 Main Street, Cambridge, MA 02142, USA. [2]Department of Medical Oncology, Dana-Farber Cancer Institute, Harvard Medical School, Boston, MA 02215, USA. [3]Department of Biology, Massachusetts Institute of Technology, Cambridge, MA 02139, USA. [4]Department of Chemical Engineering, Massachusetts Institute of Technology, Cambridge, MA 02139, USA. [5]Institute for Medical Engineering & Science, Massachusetts Institute of Technology, Cambridge, MA 02139, USA. [6]Koch Institute for Integrative Cancer Research, Massachusetts Institute of Technology, Cambridge, MA 02139, USA. [7]Laboratory of Biochemistry and Molecular Biology, The Rockefeller University, New York, NY 10065, USA. [8]Department of Physics, Massachusetts Institute of Technology, Cambridge, MA 02139, USA. [9]Department of Chemistry, Massachusetts Institute of Technology, Cambridge, MA 02139, USA. [10]Department of Biological Engineering, Massachusetts Institute of Technology, Cambridge, MA 02139, USA. [11]Ragon Institute of Massachusetts General Hospital, Massachusetts Institute of Technology and Harvard, Cambridge, MA 02139, USA.
*These authors contributed equally to this work.
†Corresponding author. Email: young@wi.mit.edu

BRD4 and MED1 coactivators form nuclear puncta

The enhancer clusters that make up SEs are occupied by master TFs and unusually high densities of factors, including BRD4 and MED1, that are coactivators (*31*–*35*) whose presence can be used to define SEs (*14*, *15*, *21*). We reasoned that if BRD4 and MED1 are components of nuclear condensates, then they might be visualized as discrete puncta in the nuclei of cells, and the properties of these puncta could be investigated. Fixed cell immunofluorescence (IF) with antibodies against BRD4 and MED1 in murine embryonic stem cells (mESCs) revealed nuclear puncta for both factors (Fig. 1A). To determine whether such puncta occur in live cells, we engineered mESCs by using CRISPR-Cas9 to tag endogenous BRD4 and MED1 with monomeric enhanced green fluorescent protein (mEGFP) (fig. S1). Live-cell fluorescence microscopy of the engineered mESC lines also revealed discrete nuclear puncta (Fig. 1B). Analysis of these images showed that there were 1034 ± 130 BRD4 and 983 ± 102 MED1 puncta per nucleus (means ± SEM) (table S1). These results demonstrate that BRD4 and MED1 are components of puncta within the nuclei of mESCs.

SEs are associated with coactivator puncta

Several lines of evidence suggest that SEs are likely to be associated with some of the BRD4 and MED1 puncta in mESCs. ChIP-seq (chromatin immunoprecipitation followed by sequencing) data for BRD4 and MED1 show that SEs are especially enriched in these coactivators (*14*, *15*). DNA interaction data suggest that SE constituents occupied by BRD4 and MED1 are in close spatial proximity to one another (Fig. 1C and fig. S2A). Co-occupancy of the genome by BRD4 and MED1 is most evident at SEs (fig. S2B) (*14*, *15*). To determine whether SEs are associated with some of the BRD4 and MED1 puncta, we performed IF for BRD4 or MED1 together with DNA-FISH or nascent RNA-FISH for the genomic region containing the *Nanog* gene and its SEs (FISH, fluorescence in situ hybridization) (Fig. 1, D to G). We found that BRD4 and MED1 puncta consistently overlapped the DNA-FISH foci (Fig. 1D) or RNA-FISH foci (Fig. 1F). An average image analysis (details are given in the methods) of the BRD4 and MED1 IF signals centered at DNA-FISH foci (n = 137 for BRD4 and 125 for MED1) and RNA-FISH foci (n = 121 for BRD4 and 181 for MED1) revealed that, on average, BRD4 and MED1 fluorescence intensities are most enriched at the center of FISH foci (Fig. 1, E and G); this trend was not observed for average images centered at randomly selected nuclear positions (Fig. 1, E and G). Radial distribution functions of the averaged images for FISH and IF pairs show a significant correlation (Spearman correlation

coefficients > 0.6; P values < 1×10^{-16}), with both BRD4 and MED1 having their highest signal intensities at the center of the FISH focus; signals decay with distance from this center (fig. S3). The radial distributions of FISH and IF at randomly selected nuclear positions are not correlated (Spearman correlation coefficients < 0.2) (fig. S3). Similar results were obtained when we performed IF for BRD4 or MED1 together with nascent RNA-FISH for the SE-regulated genes *Klf4*, *Mir290*, and *Trim28* (figs. S3 and S4, A to F). When a similar experiment was conducted for two genes expressed in mESCs but not associated with a SE (*Fam168b* and *Zfp606*), there was no evident overlap between FISH foci

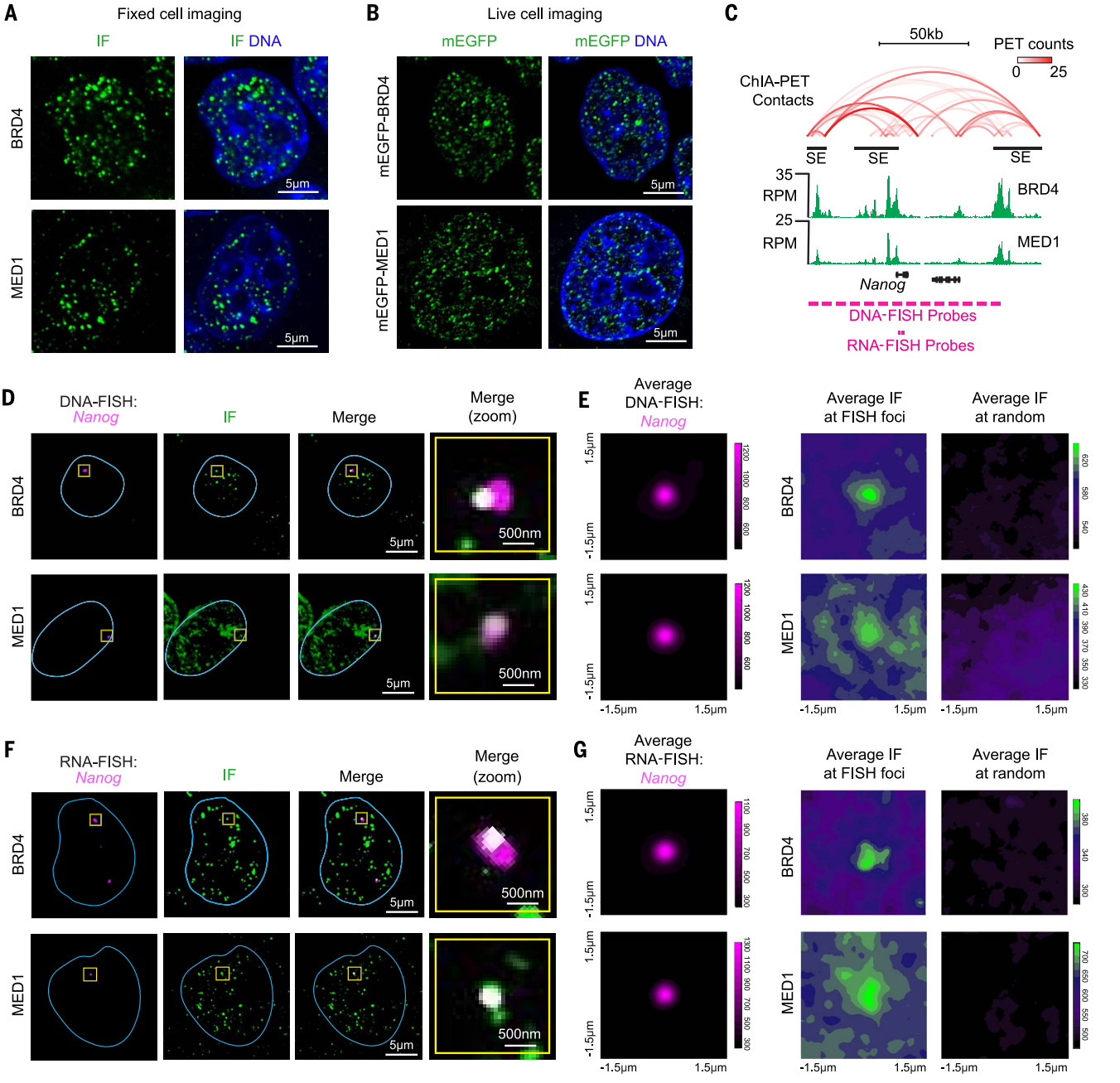

Fig. 1. BRD4 and MED1 form puncta at super-enhancers (SEs). (**A**) Immunofluorescence (IF) imaging of BRD4 and MED1 in mouse embryonic stem cells (mESCs). Fluorescence signal is shown alone (left) and merged with Hoechst stain (right). (**B**) Live imaging of endogenously tagged mEGFP-BRD4 and mEGFP-MED1 in mESCs. (**C**) Depiction of *Nanog* locus, associated SEs (black bars), DNA contacts (red arcs), BRD4 and MED1 ChIP-seq (green histograms), and location of FISH probes. ChIA-PET, chromatin interaction analysis with paired-end tag; RPM, reads per million. (**D**) Colocalization between BRD4 or MED1 and the *Nanog* locus by IF and DNA-FISH in fixed mESCs. Separate images of the indicated IF and FISH are shown, along with an image showing the merged channels (overlapping signal in white). The blue line highlights the nuclear periphery, determined by Hoechst staining (not shown). The rightmost column shows the area in the yellow box in greater detail. (**E**) Averaged signal of (left) DNA-FISH for *Nanog* and (right) IF for BRD4 or MED1 centered at *Nanog* DNA-FISH foci or randomly selected nuclear positions. (**F**) Colocalization between BRD4 or MED1 and the nascent RNA of *Nanog*, determined by IF and RNA-FISH in fixed mESCs. Data are shown as in (D). (**G**) Averaged signal of (left) RNA-FISH for *Nanog* and (right) IF for BRD4 or MED1 centered at *Nanog* RNA-FISH foci or randomly selected nuclear positions.

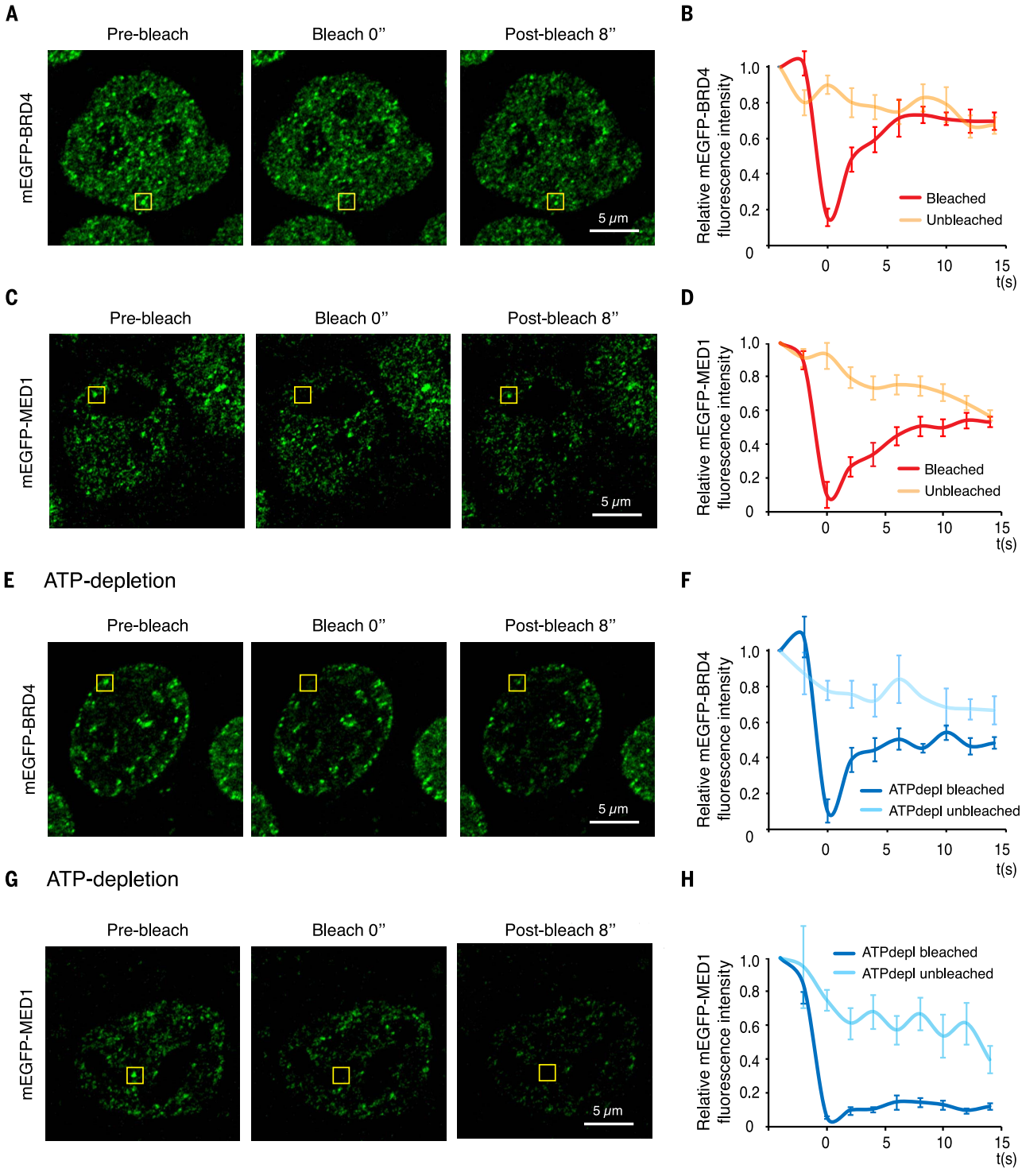

Fig. 2. BRD4 and MED1 nuclear puncta exhibit properties expected for biomolecular condensates. (**A**) Representative images of the FRAP experiment with mEGFP-BRD4–engineered mESCs (where " indicates time in seconds). The yellow box highlights the punctum undergoing targeted bleaching. (**B**) Quantification of FRAP data for mEGFP-BRD4 puncta. The bleaching event occurs at t = 0 s. For the bleached area and the unbleached control, background-subtracted fluorescence intensities are plotted relative to a prebleach time point (t = −4 s). Data are plotted as means ± SEM (n = 9). (**C**) Same as (A), but with mEGFP-MED1–engineered mESCs. (**D**) Same as (B), but for mEGFP-MED1 puncta (n = 9). (**E**) Representative images of the FRAP experiment with mEGFP-BRD4–engineered mESCs upon ATP depletion. (**F**) Quantification of FRAP data for mEGFP-BRD4 puncta upon ATP depletion (n = 8), as in (B). (**G**) Representative images of the FRAP experiment with mEGFP-MED1–engineered mESCs upon ATP depletion. (**H**) Quantification of FRAP data for mEGFP-MED1 puncta upon ATP depletion (n = 8), as in (B). Images were taken using the Zeiss LSM 880 confocal microscope with an Airyscan detector and a 63× objective at 37°C.

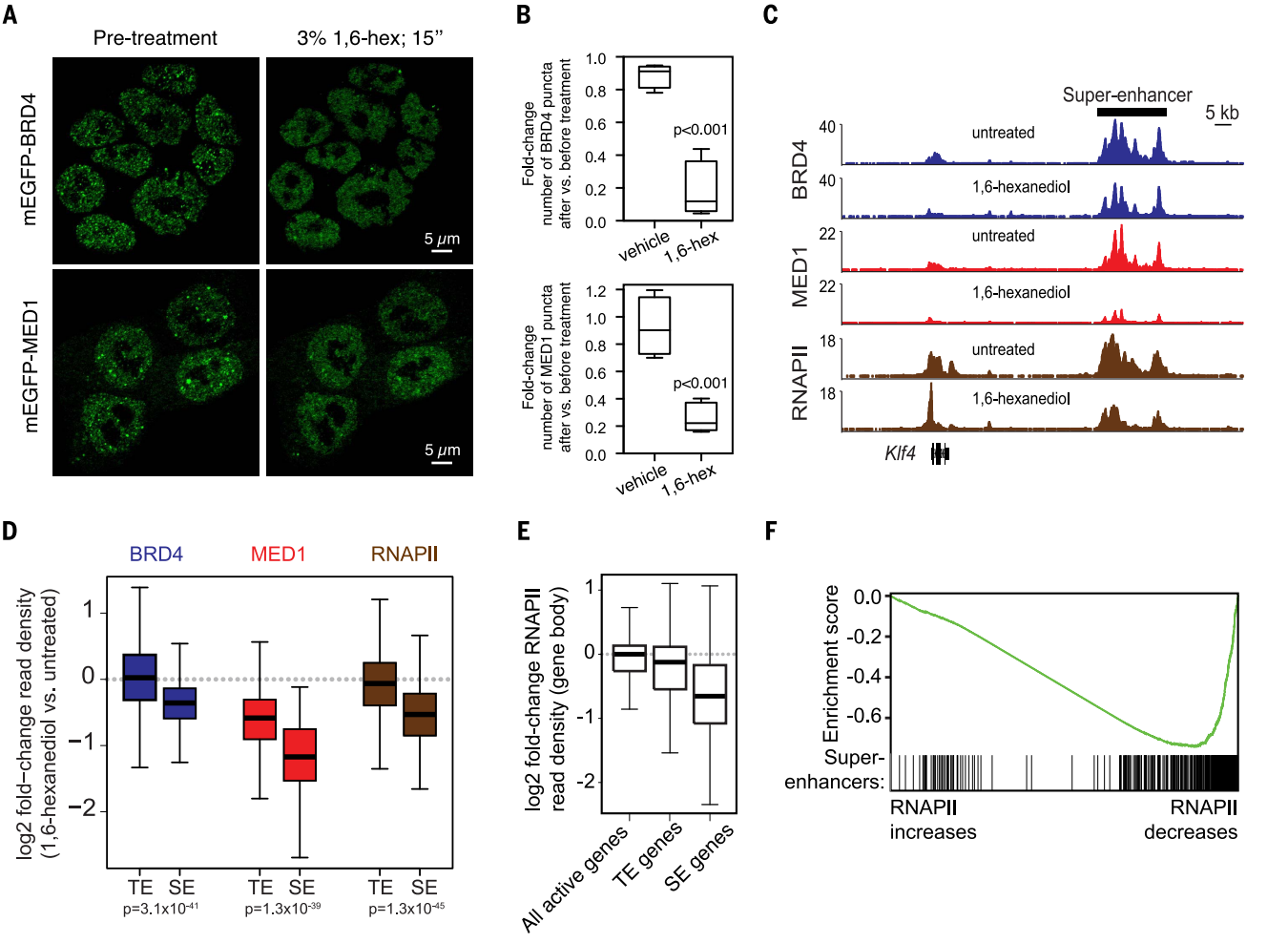

Fig. 3. 1,6-hexanediol disrupts BRD4 and MED1 puncta and disrupts BRD4, MED1, and RNA Pol II occupancy at SEs and SE-driven genes. (**A**) Representative images of mEGFP-BRD4– or mEGP-MED1–engineered mESCs before and after treatment with 3% hexanediol for 15 s. (**B**) Box-plot representation of the fold change in the number of mEGFP-BRD4 or mEGFP-MED1 puncta observed after addition of vehicle or 1,6-hexanediol to a final concentration of 3%. (**C**) Genome browser view of BRD4 (blue), MED1 (red), and RNA Pol II (RNAPII, brown) ChIP-seq data from untreated or 1,6-hexanediol–treated (1.5% for 30 min) mESCs at the *Klf4* locus. The *y* axis shows reads per million. (**D**) Box-plot representation of the log2 fold change in BRD4 (blue), MED1 (red), and RNA Pol II (brown) ChIP-seq read density (1,6-hexanediol–treated versus untreated) for regions defined as SEs or typical enhancers (TEs) (methods and table S2). (**E**) Box-plot representation of the log2 fold change in RNA Pol II ChIP-seq density (1,6-hexanediol–treated versus untreated) within the gene body (transcription start site to transcription end site) of all active genes (reads per kilobase per million > 1), TE-associated genes, or SE-associated genes. (**F**) Gene set enrichment analysis, with genes ranked by their log2 fold change in RNA Pol II ChIP-seq density within the gene body and annotated against the set of SE-associated genes. Enrichment score profile and the position of SE-associated genes are shown.

and BRD4 puncta (fig. S4G). These results indicate that both BRD4 and MED1 puncta are present at SEs.

Coactivator puncta exhibit liquid-like rates of fluorescence recovery after photobleaching

We next sought to examine whether BRD4 and MED1 puncta exhibit features characteristic of liquid-like condensates. A hallmark of liquid-like condensates is internal dynamical reorganization and rapid exchange kinetics (*1*–*3*), which can be interrogated by measuring the rate of fluorescence recovery after photobleaching (FRAP). To study the dynamics of BRD4 and MED1 foci in live cells, we performed FRAP experiments on endogenously tagged mEGFP-BRD4 or mEGFP-MED1 cell lines. After photobleaching, mEGFP-BRD4 and mEGFP-MED1 puncta recovered fluorescence on a time scale of seconds (Fig. 2, A to D), with apparent diffusion coefficients of ~0.37 ± 0.13 and ~0.14 ± 0.04 $\mu m^2/s$, respectively. These values are similar to those previously reported for components of liquid-like condensates (*36*, *37*). Adenosine triphosphate (ATP) has been implicated in promoting condensate fluidity by driving energy-dependent processes and/or through its intrinsic hydrotrope activity (*38*, *39*). Depletion of cellular ATP by glucose deprivation and oligomycin treatment altered fluorescence recovery after photobleaching for both mEGFP-BRD4 and mEGFP-MED1 foci; the rate of recovery for MED1 was reduced, and the extent of recovery for BRD4 was diminished (Fig. 2, E to H). These results indicate that puncta containing BRD4 and MED1 have liquid-like properties in cells, consistent with previously described phase-separated condensates.

Coactivator puncta and SE occupancy are sensitive to condensate perturbation

To further investigate the biophysical properties of BRD4 and MED1 puncta, we investigated their sensitivity to 1,6-hexanediol, a compound known to disrupt liquid-like condensates, possibly by disruption of hydrophobic interactions (*40*). We found that treatment of mESCs expressing endogenously tagged mEGFP-BRD4 or mEGFP-MED1

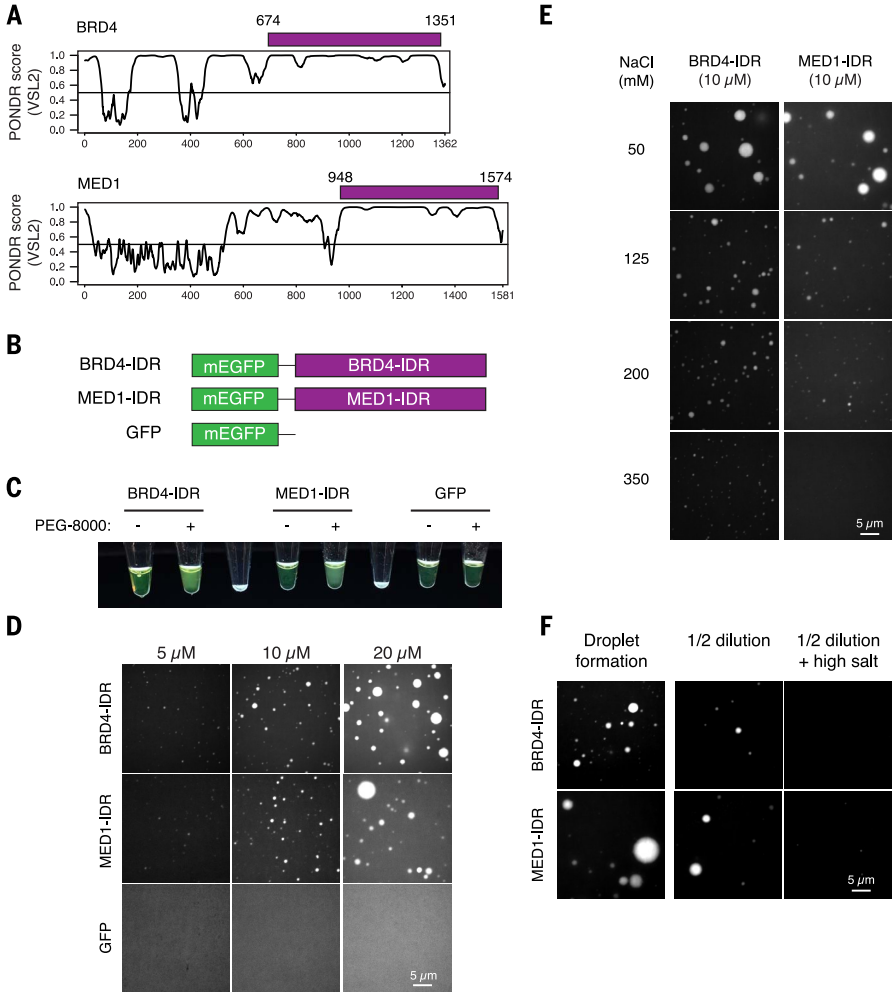

Fig. 4. Intrinsically disordered regions (IDRs) of BRD4 and MED1 phase-separate in vitro. (**A**) Graphs plotting intrinsic disorder for BRD4 and MED1. PONDR (Predictor of Natural Disordered Regions) VSL2 scores are shown on the *y* axis, and amino acid positions are shown on the *x* axis. The purple bar designates the IDR under investigation. (**B**) Schematic of recombinant mEGFP fusion proteins used in this study. Purple boxes indicate the IDRs of BRD4 and MED1 shown in (A). (**C**) Visualization of turbidity associated with droplet formation. Tubes containing BRD4-IDR (left pair), MED1-IDR (middle pair), or GFP (right pair) in the presence (+) or absence (−) of PEG-8000 are shown. Blank tubes are included between pairs for contrast. (**D**) Representative images of droplet formation at different protein concentrations. BRD4-IDR, MED1-IDR, or mEGFP were added to the droplet formation buffer to the final concentrations indicated. (**E**) Representative images of droplet formation at different salt concentrations. BRD4-IDR or MED1-IDR was added to droplet formation buffer to achieve 10 μM protein concentration with a final NaCl concentration as indicated. (**F**) Representative images of the droplet reversibility experiment with BRD4-IDR (top row) or MED1-IDR (bottom row) [20 μM protein and 75 mM NaCl (initial), followed by a 1:1 dilution (1/2 dilution) or a 1:1 dilution with an increase to 425 mM NaCl (1/2 dilution + NaCl)].

with 1,6-hexanediol caused a reduction in the number of BRD4 and MED1 puncta (Fig. 3, A and B).

To determine the effect of 1,6-hexanediol on BRD4, MED1, and RNA polymerase II (RNA Pol II) occupancy at enhancers and genes, ChIP-seq was performed with antibodies against these proteins in untreated or 1,6-hexanediol–treated mESCs. Treatment with 1,6-hexanediol caused a reduction in all three proteins at enhancers, with the most profound effects occurring at SEs (Fig. 3, C and D, and fig. S5A). For example, at the *Klf4* SE, the levels of BRD4 were reduced by 44%, those of MED1 by 80%, and those of RNA Pol II by 56% (Fig. 3C). Similar effects were observed genome-wide, where reductions in BRD4, MED1, and RNA Pol II were substantially larger at SEs than at typical enhancers (Fig. 3D), and the degrees to which BRD4 and MED1 were lost from SEs were positively correlated (fig. S5B). These results are consistent with the notion that BRD4 and MED1 form condensates at SEs that are sensitive to 1,6-hexanediol.

The level of RNA Pol II occupancy across gene bodies can be used as a measure of transcriptional output (*41*). The ChIP-seq data revealed that the reduction in BRD4 and MED1 occupancy at SEs was associated with a loss of RNA Pol II occupancy across SE-associated gene bodies (Fig. 3, C and E, and fig. S5A). When genes were ranked by the extent to which RNA Pol II was lost upon 1,6-hexanediol treatment, SE-associated genes were highly enriched among those that lost the most RNA Pol II (Fig. 3F). These results are consistent with the idea that BRD4 and MED1 condensates are associated with SEs and that loss of condensate integrity adversely affects transcription.

IDRs of BRD4 and MED1 phase-separate in vitro

BRD4 and MED1 contain large IDRs (Fig. 4A) and share features with the IDRs of several proteins known to facilitate condensate formation (*2*, *3*), including high proline and glutamine content (BRD4), high serine content (MED1), and acidic and basic regions (BRD4 and MED1). The purified IDRs of several proteins involved in

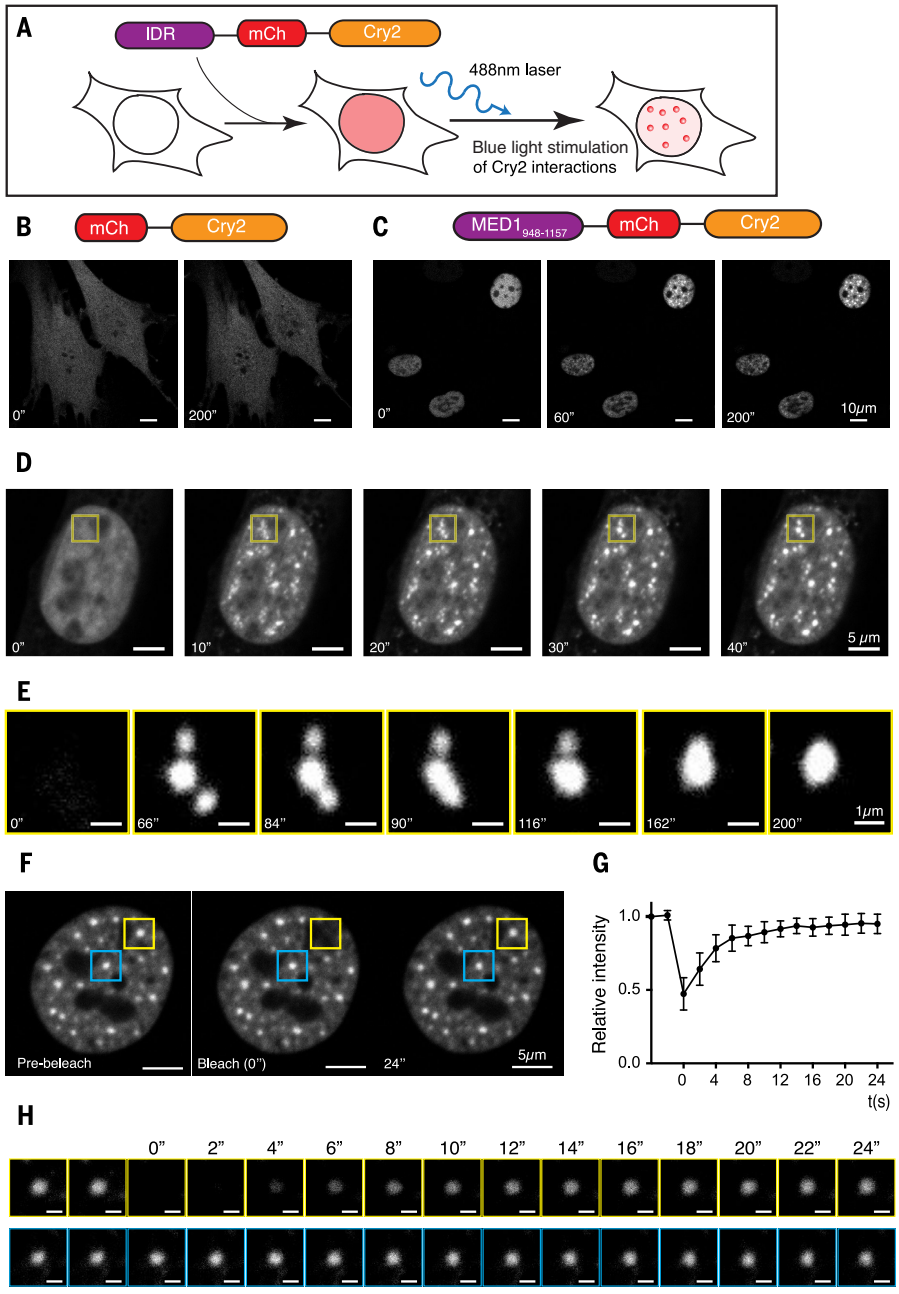

Fig. 5. The IDR of MED1 participates in phase separation in cells. (**A**) Schematic of the optoIDR assay, depicting recombinant protein with an IDR (purple), mCherry (red), and Cry2 (orange) expressed in cells exposed to blue light. (**B** and **C**) Images of NIH3T3 cells expressing either (B) mCherry-Cry2 or (C) a portion of the MED1-IDR (amino acids 948 to 1157) fused to mCherry-Cry2 (MED1-optoIDR). Cells were subjected to laser excitation every 2 s for the indicated times. (**D**) Time-lapse images of the nucleus of an NIH3T3 cell expressing MED1-optoIDR subjected to laser excitation every 2 s for the times indicated. A droplet fusion event occurs in the region highlighted by the yellow box. (**E**) The droplet fusion event highlighted in (D) at higher resolution and extended times as indicated. (**F**) Image of a MED1-optoIDR optoDroplet (yellow box) before (left), during (middle), and after (right) photobleaching. The blue box highlights an unbleached region for comparison. Time relative to photobleaching (0 s) is indicated. (**G**) Signal intensity relative to the prebleaching signal (*y* axis) versus time relative to photobleaching (*x* axis). Data are shown as average relative intensity ± SD (n = 15). (**H**) Time-lapse and close-up view of droplet recovery for regions highlighted in (F). Times relative to photobleaching are indicated. Scale bars, 1 μm.

condensate formation form phase-separated droplets in vitro (*7*, *36*, *37*, *42*), so we investigated whether the IDRs of BRD4 or MED1 form such droplets in vitro. Purified recombinant mEGFP-IDR fusion proteins (BRD4-IDR and MED1-IDR) (Fig. 4B) were added to buffers containing 10% PEG-8000 (polyethylene glycol, molecular weight 8000; materials and methods), turning the solution opaque, whereas equivalent solutions with mEGFP alone remained clear (Fig. 4C). Fluorescence microscopy of the opaque MED1-IDR and BRD4-IDR solutions revealed GFP-positive, micron-sized spherical droplets freely moving in solution (Movies 1 and 2) and falling onto and wetting the surface of the glass coverslip, where they remained stationary (Movie 3). As determined by aspect ratio analysis, the MED1-IDR and BRD4-IDR droplets were highly spherical (fig. S6A), a property expected for liquid-like droplets (*1*–*3*).

Phase-separated droplets typically scale in size according to the concentration of components in the system (*43*). We performed the droplet formation assay with varying concentrations of BRD4-IDR, MED1-IDR, and mEGFP, ranging from 0.625 to 20 μM. BRD4-IDR and MED1-IDR formed droplets with concentration-dependent size distributions, whereas mEGFP remained diffuse in all conditions tested (Fig. 4D and fig. S6B). Although these droplets were smaller at lower concentrations, we observed BRD4-IDR and MED1-IDR droplets at the lowest concentration tested (0.625 μM) (fig. S6C).

To investigate the biophysical properties of these droplets, we tested their ability to form under varying salt concentrations (to probe the contribution of electrostatic interactions) or upon 1,6-hexanediol treatment (to probe the contribution of hydrophobic interactions). The size distributions of both BRD4-IDR and MED1-IDR droplets shifted toward smaller droplets with increasing NaCl concentration (from 50 to 350 mM) (Fig. 4E and fig. S6D), and opacity was reduced with 10% 1,6-hexanediol treatment (fig. S7A). These results demonstrate that a variety of molecular interactions contribute to BRD4-IDR and MED1-IDR droplet formation.

We next sought to test whether the droplets are irreversible aggregates or reversible phase-separated condensates. To do this, BRD4-IDR and MED1-IDR were allowed to form droplets in an initial solution. The protein concentration was then diluted by half in equimolar salt or in

a higher salt solution (Fig. 4F). The preformed BRD4-IDR and MED1-IDR droplets were reduced in size and number with dilution and even further reduced with elevated salt concentration (Fig. 4F and fig. S7B). These results show that the BRD4-IDR and MED1-IDR droplets form a distribution of sizes that is dependent on the conditions of the system and, once formed, respond to changes in the system, with rapid adjustments in size. These features are characteristic of phase-separated condensates formed by networks of weak protein-protein interactions (*1*–*3*).

MED1-IDR participates in liquid-liquid phase separation in cells

To investigate whether the coactivator IDRs facilitate phase separation in cells, we used a previously developed assay to manipulate local protein concentrations within the cell; this optoIDR assay tests IDR-dependent, light-inducible droplet formation in vivo (*44*). Briefly, the photoactivatable, self-associating Cry2 protein was labeled with mCherry and fused to an IDR of interest. This fusion mediates a blue light–inducible increase in the local concentration of selected IDRs within the cell (Fig. 5A) (*44*). In this assay, IDRs known to promote phase separation enhance the photoresponsive clustering properties of Cry2 (*45*, *46*), causing rapid formation of liquid-like spherical droplets under stimulation by blue light. Fusion of a portion of the MED1-IDR to Cry2-mCherry facilitated the rapid formation of micron-sized spherical droplets upon blue light stimulation (optoDroplets) (Fig. 5, B and C, and fig. S8). During stimulation, proximal droplets were observed to fuse (Fig. 5, D and E, and Movie 4). The fusions exhibited characteristic liquid-like fusion properties of necking and relaxation to spherical shape (Fig. 5E). The MED1-IDR droplets persisted after blue light stimulation and exhibited liquid-like FRAP recovery rates in the absence of blue light stimulation (Fig. 5, F to H). The rapid FRAP kinetics in the absence of light-activated Cry2 interactions suggests that the MED1-IDR optoDroplets established by blue light are dynamic assemblies exchanging with the dilute phase.

Conserved serine bias in the MED1-IDR is necessary for phase separation

Previous studies have implicated low-complexity IDRs of proteins in liquid-liquid phase separation (*7*, *36*, *37*, *42*). An examination of the amino acid content of MED1 revealed that the IDR contains a compositional bias for serine (Fig. 6A). This serine compositional bias is conserved among vertebrates (Fig. 6B). To investigate whether the serine bias is necessary for the MED1-IDR's capacity to phase-separate, we mutated all the serine (S) residues to alanine (A) and investigated the ability of this mutated IDR to form phase-separated droplets in vitro. The MED1-IDR S-to-A mutant was incapable of forming phase-separated droplets under conditions in which the wild-type IDR readily formed droplets (Fig. 6C), indicating that the conserved serine bias in the MED1-IDR is necessary for droplet formation.

MED1-IDR droplets can incorporate proteins necessary for transcription

A proposed function of phase separation at SEs is the ability to compartmentalize and concentrate factors within a biomolecular condensate, so we sought to test whether MED1-IDR droplets could recapitulate this compartmentalization function in vitro. We identified conditions under which the MED1-IDR could form droplets but the BRD4-IDR could not (fig. S9). We then investigated whether the MED1-IDR droplets could compartmentalize BRD4-IDR protein under these conditions (Fig. 7A). Using differentially labeled proteins (mCherry–MED1-IDR and mEGFP–BRD4-IDR), we found that the MED1-IDR droplets could incorporate, and thus concentrate, the BRD4-IDR protein (Fig. 7A). The MED1-IDR droplets did not incorporate mEGFP (Fig. 7A). To probe the approximate mesh size of the MED1-IDR droplets (*47*), we incubated them with fluorescently labeled dextrans with average molecular weights of 4, 10, and 40 kDa. We found that the 4-kDa dextrans were incorporated into the MED1-IDR droplets, the 10-kDa dextrans were incorporated with less efficiency, and the 40-kDa dextrans were excluded (fig. S10). These results suggest that the incorporation of mEGFP–BRD4-IDR (105 kDa) into the MED1-IDR droplet is due to attractive molecular interactions, as opposed to passive diffusion through the droplet mesh.

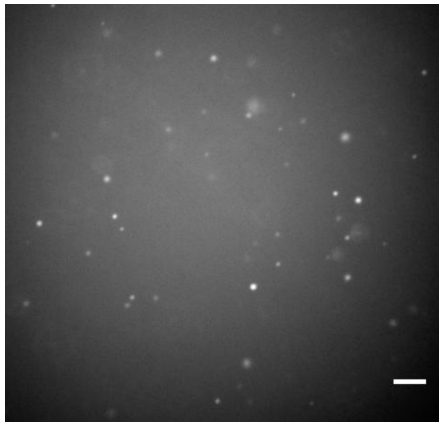

Movie 1. BRD4-IDR droplets in solution. Each frame represents 1 s. The movie is rendered at 12 frames per second. 20 μM protein, 125 mM NaCl. Scale bar, 5 μm.

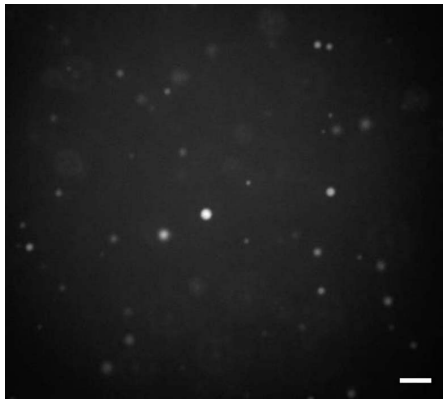

Movie 2. MED1-IDR droplets in solution. Each frame represents 1 s. The movie is rendered at 12 frames per second. 20 μM protein, 125 mM NaCl. Scale bar, 5 μm.

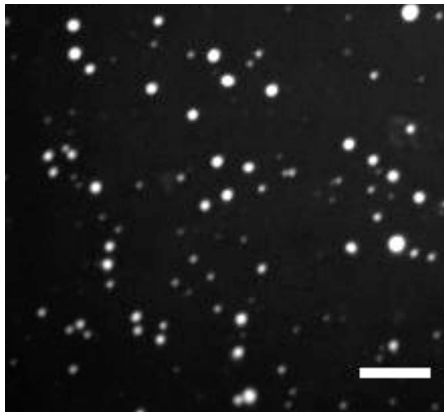

Movie 3. MED1-IDR droplets settling onto a glass coverslip. Each frame represents 1 s. The movie is rendered at 12 frames per second. 10 μM protein, 125 mM NaCl. Scale bar, 5 μm.

We next investigated whether the MED1-IDR, introduced into a transcription-competent nuclear extract, would form droplets that might incorporate BRD4 or other transcriptional components. We found that the wild-type MED1-IDR, but not the MED1-IDR S-to-A mutant, formed droplets in these extracts (Fig. 7B). The MED1-IDR phase-separated droplets were denser than the surrounding extract and thus could be purified from solution by centrifugation. Immunoblot analysis revealed that BRD4 and the largest subunit of RNA Pol II (RPB1) were enriched in pelleted droplets in a MED1-IDR dose–dependent manner (Fig. 7C). These results indicate that the MED1-IDR droplets can incorporate BRD4 and RNA Pol II.

The ability of the MED1-IDR protein to incorporate BRD4 and RNA Pol II into an artificial phase-separated compartment suggests that it sequesters key components of the transcription apparatus and might thus "squelch" transcription in the nuclear extract. We carried out an in vitro transcription assay with these extracts and found that the wild-type MED1-IDR protein does squelch transcription, correlating with the amount of material separated from solution by the MED1-IDR droplets (Fig. 7D). We did not observe these effects with equivalent concentrations of mEGFP or with the MED1-IDR S-to-A mutant (Fig. 7D). These results demonstrate that the MED1-IDR has the capacity to compartmentalize and concentrate transcriptional machinery from a complex nuclear extract.

Discussion

SEs regulate genes with prominent roles in healthy and diseased cellular states (*14*, *15*, *19*–*25*, *48*, *49*). SEs and their components have been proposed to form phase-separated condensates (*30*), but with no direct evidence. Here we demonstrate that two key components of SEs, BRD4 and MED1, form nuclear condensates at sites of SE-driven

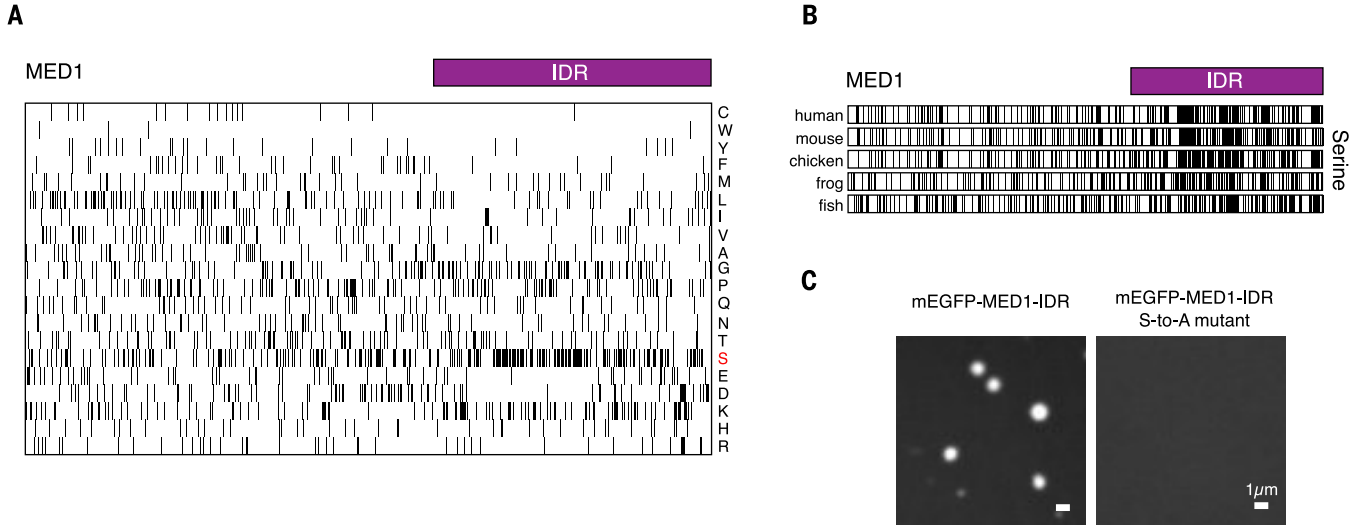

Fig. 6. Conserved serine bias is necessary for MED1-IDR phase separation. (**A**) Amino acid composition of the MED1 protein. Each row represents information for a single amino acid. Single-letter amino code abbreviations (right) are as follows: A, Ala; C, Cys; D, Asp; E, Glu; F, Phe; G, Gly; H, His; I, Ile; K, Lys; L, Leu; M, Met; N, Asn; P, Pro; Q, Gln; R, Arg; S, Ser; T, Thr; V, Val; W, Trp; and Y, Tyr. The length of the row corresponds to the length of the MED1 protein. Black bars represent the occurrence of the indicated amino acid at that position in MED1. The purple bar represents the IDR of MED1 under investigation. (**B**) Serine composition of MED1 protein from indicated organisms, presented as in (A). (**C**) Mutating all serines to alanine (S to A) disrupts phase separation. Representative images of wild-type MED1-IDR or MED1-IDR S-to-A mutant fused to mEGFP in the droplet formation assay (10 μM protein, 125 mM NaCl, and 10% Ficoll-400).

transcription. Within these condensates, BRD4 and MED1 exhibit apparent diffusion coefficients similar to those previously reported for other proteins in phase-separated condensates in vivo (*36*, *37*). The IDRs of both BRD4 and MED1 are sufficient to form phase-separated droplets in vitro, and the MED1-IDR facilitates phase separation in living cells. Droplets formed by MED1-IDR are capable of concentrating transcriptional machinery in a transcriptionally competent nuclear extract. These results support a model in which transcriptional coactivators form phase-separated condensates that compartmentalize and concentrate the transcription apparatus at SE-regulated genes and identify SE components that likely play a role in phase separation.

SEs are established by the binding of master TFs to enhancer clusters (*14*, *15*). These TFs typically consist of a structured DNA-binding domain and an intrinsically disordered transcriptional activation domain (*50*–*52*). The activation domains of these TFs recruit high densities of many transcription proteins, which, as a class, are enriched for IDRs (*53*). Although the exact client-scaffold relationship (*54*) between these components remains unknown, it is likely that these protein sequences mediate weak multivalent interactions, thereby facilitating condensation. We propose that condensation of such high-valency factors at SEs creates a reaction crucible within the separated dense phase, where high local concentrations of the transcriptional machinery ensure robust gene expression.

The nuclear organization of chromosomes is likely influenced by condensates at SEs. DNA interaction technologies indicate that the individual enhancers within the SEs have exceptionally high interaction frequencies with one another (*16*–*18*), consistent with the idea that condensates draw these elements into close proximity in the dense phase. Several recent studies suggest that SEs can interact with one another and may also contribute in this fashion to chromosome organization (*55*, *56*). Cohesin, an SMC (structural maintenance of chromosomes) protein complex, has been implicated in constraining SE-SE interactions because its loss causes extensive fusion of SEs within the nucleus (*56*). These SE-SE interactions may be due to a tendency of liquid-phase condensates to undergo fusion (*1*–*3*).

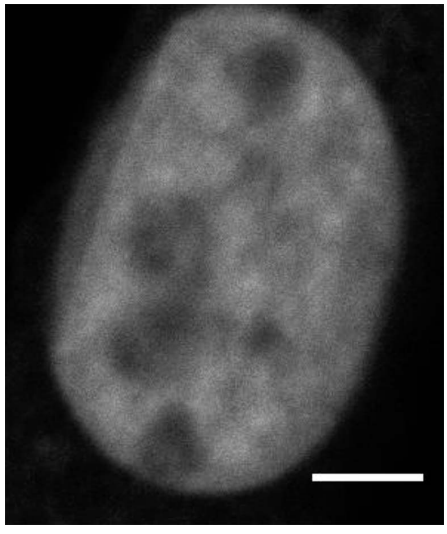

Movie 4. Formation of MED1-IDR optoDroplets upon stimulation with blue light. NIH3T3 cells expressing the MED1-optoIDR construct were subjected to 488-nm laser light in 2-s intervals. Each frame represents 2 s. The movie is rendered at 12 frames per second. Scale bar, 5 μm.

The model whereby phase separation of coactivators compartmentalizes and concentrates the transcription apparatus at SEs and their regulated genes, described here and corroborated by (*57*), raises many questions. How does condensation contribute to regulation of transcriptional output? A study of RNA Pol II clusters, which may be phase-separated condensates, suggests a positive correlation between condensate lifetime and transcriptional output (*58*). What components drive formation and dissolution of transcriptional condensates? Our studies indicate that BRD4 and MED1 likely participate, but the roles of DNA-binding TFs, RNA Pol II, and regulatory RNAs require further study. Why do some proteins, such as HP1a, contribute to phase-separated heterochromatin condensates (*59*, *60*) and others contribute to euchromatic condensates? The rules that govern partitioning into specific types of condensates have begun to be studied (*61*–*65*) and will need to be defined for proteins involved in transcriptional condensates. Does condensate misregulation contribute to pathological processes in disease, and will new insights into condensate behaviors present new opportunities for therapy? Mutations within IDRs and misregulation of phase separation have already been implicated in a number of neurodegenerative diseases (*66*–*68*). Tumor cells have exceptionally large SEs at driver oncogenes that are not found in their cell of origin, and some of these are exceptionally sensitive to drugs that target SE components (*22*–*25*). How do we take advantage of phase separation

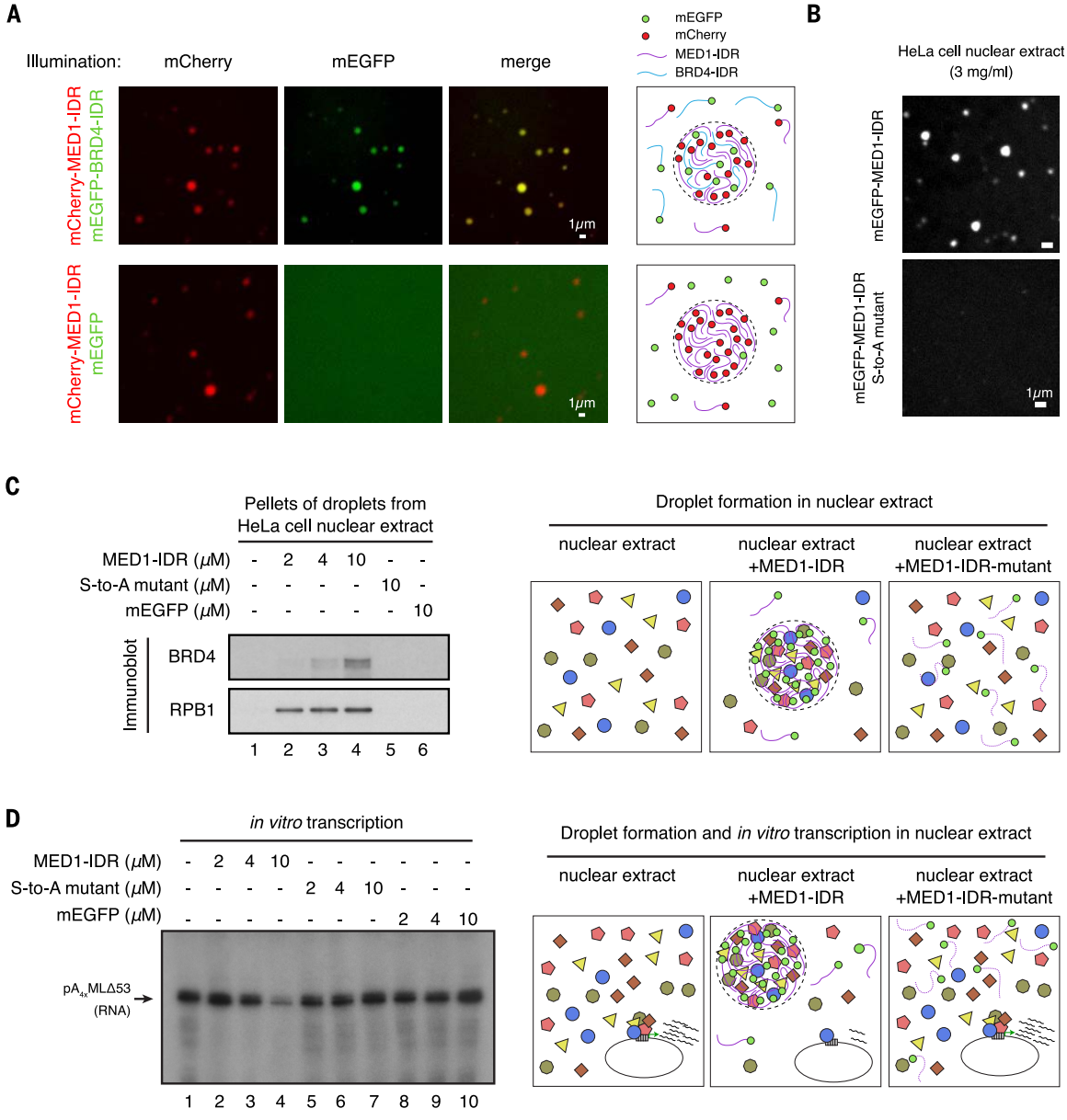

Fig. 7. MED1-IDR droplets compartmentalize and concentrate proteins necessary for transcription. (**A**) MED1-IDR droplets incorporate BRD4-IDR protein in vitro. The indicated mEGFP or mCherry fusion proteins were mixed at 10 μM each in buffer D containing 10% Ficoll-400 and 125 mM NaCl. Indicated fluorescence channels are presented for each mixture. Illustrations summarizing results are shown on the right. (**B**) MED1-IDR forms droplets in an in vitro transcription reaction containing HeLa cell nuclear extract, whereas the MED1-IDR S-to-A mutant does not. Shown are representative images of the indicated mEGFP-fusion protein when added to an in vitro transcription reaction containing HeLa cell nuclear extract at a final concentration of 3 mg/ml (a complete list of components is given in the methods). (**C**) MED1-IDR droplets compartmentalize transcriptional machinery from a nuclear extract. Shown are immunoblots of the pellet fraction of the indicated protein added to in vitro transcription reactions [as described in (B)]. A proposed model of molecular interactions taking place within MED1-IDR droplets in the nuclear extract is illustrated on the right. (**D**) MED1-IDR droplets compartmentalize machinery necessary for the in vitro transcription reaction. An autoradiograph of radiolabeled RNA products of in vitro transcription reactions under indicated conditions is shown on the left. The arrow indicates the expected RNA product. Reactions were conducted as in (*68*) with minor modifications (full details are given in the methods). A proposed model of molecular interactions taking place within MED1-IDR droplets in nuclear extract and the impact on the in vitro transcription reaction is illustrated on the right.

principles established in physics and chemistry to more effectively improve our understanding of this form of regulatory biology? Addressing these questions at the crossroads of physics, chemistry, and biology will require collaboration across these diverse sciences.

Methods summary

Immunofluorescence against BRD4 and MED1, coupled with DNA-FISH or RNA-FISH against SEs or SE-driven nascent transcripts, was performed in mESCs to visualize the colocalization between BRD4 or MED1 puncta and SEs. BRD4 and MED1 were endogenously tagged with mEGFP in mESCs to visualize the organization of BRD4 and MED1 and to study their dynamics by FRAP and drug treatments in live cells. ChIP-seq was performed to investigate the effect of 1,6-hexanediol treatment on the chromatin occupancy of BRD4, MED1, and RNA Pol II. Recombinant BRD4-IDR and MED1-IDR were purified to test their capacity to phase-separate in vitro. The optoIDR assay (*45*) was implemented to test the capacity of a section of MED1-IDR to phase-separate in live cells. Mutations were introduced into MED1-IDR to study the sequence determinants of MED1-IDR phase separation. BRD4-IDR and MED1-IDR fused to different fluorescent tags were used to demonstrate the capacity of MED1-IDR droplets to compartmentalize and concentrate BRD4-IDR. Formation of MED1-IDR droplets in a transcriptionally competent nuclear extract was used to study the ability of MED1-IDR droplets to compartmentalize and concentrate BRD4 and RNA Pol II from a complex extract. In vitro transcription assays were used to measure the effect of synthetic droplet formation on transcription. All procedures are described in detail in the supplementary materials.

REFERENCES AND NOTES

1. A. A. Hyman, C. A. Weber, F. Jülicher, Liquid-liquid phase separation in biology. *Annu. Rev. Cell Dev. Biol.* **30**, 39–58 (2014). doi: 10.1146/annurev-cellbio-100913-013325; pmid: 25288112
2. S. F. Banani, H. O. Lee, A. A. Hyman, M. K. Rosen, Biomolecular condensates: Organizers of cellular biochemistry. *Nat. Rev. Mol. Cell Biol.* **18**, 285–298 (2017). doi: 10.1038/nrm.2017.7; pmid: 28225081
3. Y. Shin, C. P. Brangwynne, Liquid phase condensation in cell physiology and disease. *Science* **357**, eaaf4382 (2017). doi: 10.1126/science.aaf4382; pmid: 28935776
4. C. P. Brangwynne *et al*., Germline P granules are liquid droplets that localize by controlled dissolution/condensation. *Science* **324**, 1729–1732 (2009). doi: 10.1126/science.1172046; pmid: 19460965
5. M. Kato *et al*., Cell-free formation of RNA granules: Low complexity sequence domains form dynamic fibers within hydrogels. *Cell* **149**, 753–767 (2012). doi: 10.1016/j.cell.2012.04.017; pmid: 22579281
6. P. Li *et al*., Phase transitions in the assembly of multivalent signalling proteins. *Nature* **483**, 336–340 (2012). doi: 10.1038/nature10879; pmid: 22398450
7. Y. Lin, D. S. W. Protter, M. K. Rosen, R. Parker, Formation and Maturation of Phase-Separated Liquid Droplets by RNA-Binding Proteins. *Mol. Cell* **60**, 208–219 (2015). doi: 10.1016/j.molcel.2015.08.018; pmid: 26412307
8. K. Adelman, J. T. Lis, Promoter-proximal pausing of RNA polymerase II: Emerging roles in metazoans. *Nat. Rev. Genet.* **13**, 720–731 (2012). doi: 10.1038/nrg3293; pmid: 22986266
9. M. Bulger, M. Groudine, Functional and mechanistic diversity of distal transcription enhancers. *Cell* **144**, 327–339 (2011). doi: 10.1016/j.cell.2011.01.024; pmid: 21295696
10. E. Calo, J. Wysocka, Modification of enhancer chromatin: What, how, and why? *Mol. Cell* **49**, 825–837 (2013). doi: 10.1016/j.molcel.2013.01.038; pmid: 23473601
11. F. Spitz, E. E. M. Furlong, Transcription factors: From enhancer binding to developmental control. *Nat. Rev. Genet.* **13**, 613–626 (2012). doi: 10.1038/nrg3207; pmid: 22868264
12. W. Xie, B. Ren, Developmental biology. Enhancing pluripotency and lineage specification. *Science* **341**, 245–247 (2013). doi: 10.1126/science.1236254; pmid: 23869010
13. M. Levine, C. Cattoglio, R. Tjian, Looping back to leap forward: Transcription enters a new era. *Cell* **157**, 13–25 (2014). doi: 10.1016/j.cell.2014.02.009; pmid: 24679523
14. W. A. Whyte *et al*., Master transcription factors and mediator establish super-enhancers at key cell identity genes. *Cell* **153**, 307–319 (2013). doi: 10.1016/j.cell.2013.03.035; pmid: 23582322
15. D. Hnisz *et al*., Super-enhancers in the control of cell identity and disease. *Cell* **155**, 934–947 (2013). doi: 10.1016/j.cell.2013.09.053; pmid: 24119843
16. J. M. Dowen *et al*., Control of cell identity genes occurs in insulated neighborhoods in mammalian chromosomes. *Cell* **159**, 374–387 (2014). doi: 10.1016/j.cell.2014.09.030; pmid: 25303531
17. D. Hnisz *et al*., Activation of proto-oncogenes by disruption of chromosome neighborhoods. *Science* **351**, 1454–1458 (2016). doi: 10.1126/science.aad9024; pmid: 26940867
18. X. Ji *et al*., 3D Chromosome Regulatory Landscape of Human Pluripotent Cells. *Cell Stem Cell* **18**, 262–275 (2016). doi: 10.1016/j.stem.2015.11.007; pmid: 26686465
19. M. R. Mansour *et al*., An oncogenic super-enhancer formed through somatic mutation of a noncoding intergenic element. *Science* **346**, 1373–1377 (2014). doi: 10.1126/science.1259037; pmid: 25394790
20. J. D. Brown *et al*., NF-κB directs dynamic super enhancer formation in inflammation and atherogenesis. *Mol. Cell* **56**, 219–231 (2014). doi: 10.1016/j.molcel.2014.08.024; pmid: 25263595
21. B. Chapuy *et al*., Discovery and characterization of super-enhancer-associated dependencies in diffuse large B cell lymphoma. *Cancer Cell* **24**, 777–790 (2013). doi: 10.1016/j.ccr.2013.11.003; pmid: 24332044
22. J. Lovén *et al*., Selective inhibition of tumor oncogenes by disruption of super-enhancers. *Cell* **153**, 320–334 (2013). doi: 10.1016/j.cell.2013.03.036; pmid: 23582323
23. E. Chipumuro *et al*., CDK7 inhibition suppresses super-enhancer-linked oncogenic transcription in MYCN-driven cancer. *Cell* **159**, 1126–1139 (2014). doi: 10.1016/j.cell.2014.10.024; pmid: 25416950
24. N. Kwiatkowski *et al*., Targeting transcription regulation in cancer with a covalent CDK7 inhibitor. *Nature* **511**, 616–620 (2014). doi: 10.1038/nature13393; pmid: 25043025
25. Y. Wang *et al*., CDK7-dependent transcriptional addiction in triple-negative breast cancer. *Cell* **163**, 174–186 (2015). doi: 10.1016/j.cell.2015.08.063; pmid: 26406377
26. D. Hnisz *et al*., Convergence of developmental and oncogenic signaling pathways at transcriptional super-enhancers. *Mol. Cell* **58**, 362–370 (2015). doi: 10.1016/j.molcel.2015.02.014; pmid: 25801169
27. T. Jiang *et al*., Identification of multi-loci hubs from 4C-seq demonstrates the functional importance of simultaneous interactions. *Nucleic Acids Res.* **44**, 8714–8725 (2016). doi: 10.1093/nar/gkw568; pmid: 27439714
28. C. Proudhon *et al*., Active and Inactive Enhancers Cooperate to Exert Localized and Long-Range Control of Gene Regulation. *Cell Rep.* **15**, 2159–2169 (2016). pmid: 27239026
29. H. Y. Shin *et al*., Hierarchy within the mammary STAT5-driven *Wap* super-enhancer. *Nat. Genet.* **48**, 904–911 (2016). doi: 10.1038/ng.3606; pmid: 27376239
30. D. Hnisz, K. Shrinivas, R. A. Young, A. K. Chakraborty, P. A. Sharp, A Phase Separation Model for Transcriptional Control. *Cell* **169**, 13–23 (2017). doi: 10.1016/j.cell.2017.02.007; pmid: 28340338
31. Z. Yang *et al*., Recruitment of P-TEFb for stimulation of transcriptional elongation by the bromodomain protein Brd4. *Mol. Cell* **19**, 535–545 (2005). doi: 10.1016/j.molcel.2005.06.029; pmid: 16109377
32. M. K. Jang *et al*., The bromodomain protein Brd4 is a positive regulatory component of P-TEFb and stimulates RNA polymerase II-dependent transcription. *Mol. Cell* **19**, 523–534 (2005). doi: 10.1016/j.molcel.2005.06.027; pmid: 16109376
33. R. Di Micco *et al*., Control of embryonic stem cell identity by BRD4-dependent transcriptional elongation of super-enhancer-associated pluripotency genes. *Cell Rep.* **9**, 234–247 (2014). pmid: 25263550
34. J. Soutourina, S. Wydau, Y. Ambroise, C. Boschiero, M. Werner, Direct interaction of RNA polymerase II and mediator required for transcription in vivo. *Science* **331**, 1451–1454 (2011). doi: 10.1126/science.1200188; pmid: 21415355
35. J. Soutourina, Transcription regulation by the Mediator complex. *Nat. Rev. Mol. Cell Biol.* **19**, 262–274 (2018). pmid: 29209056
36. T. J. Nott *et al*., Phase transition of a disordered nuage protein generates environmentally responsive membraneless organelles. *Mol. Cell* **57**, 936–947 (2015). doi: 10.1016/j.molcel.2015.01.013; pmid: 25747659
37. C. W. Pak *et al*., Sequence Determinants of Intracellular Phase Separation by Complex Coacervation of a Disordered Protein. *Mol. Cell* **63**, 72–85 (2016). doi: 10.1016/j.molcel.2016.05.042; pmid: 27392146
38. C. P. Brangwynne, T. J. Mitchison, A. A. Hyman, Active liquid-like behavior of nucleoli determines their size and shape in Xenopus laevis oocytes. *Proc. Natl. Acad. Sci. U.S.A.* **108**, 4334–4339 (2011). doi: 10.1073/pnas.1017150108; pmid: 21368180
39. A. Patel *et al*., ATP as a biological hydrotrope. *Science* **356**, 753–756 (2017). doi: 10.1126/science.aaf6846; pmid: 28522535
40. S. Kroschwald, S. Maharana, A. Simon, Hexanediol: A chemical probe to investigate the material properties of membrane-less compartments. *Matters* 10.19185/matters.201702000010 (2017).
41. C. Y. Lin *et al*., Transcriptional amplification in tumor cells with elevated c-Myc. *Cell* **151**, 56–67 (2012). doi: 10.1016/j.cell.2012.08.026; pmid: 23021215
42. S. Elbaum-Garfinkle *et al*., The disordered P granule protein LAF-1 drives phase separation into droplets with tunable viscosity and dynamics. *Proc. Natl. Acad. Sci. U.S.A.* **112**, 7189–7194 (2015). doi: 10.1073/pnas.1504822112; pmid: 26015579
43. C. P. Brangwynne, Phase transitions and size scaling of membrane-less organelles. *J. Cell Biol.* **203**, 875–881 (2013). doi: 10.1083/jcb.201308087; pmid: 24368804
44. Y. Shin *et al*., Spatiotemporal Control of Intracellular Phase Transitions Using Light-Activated optoDroplets. *Cell* **168**, 159–171.e14 (2017). doi: 10.1016/j.cell.2016.11.054; pmid: 28041848
45. I. Ozkan-Dagliyan *et al*., Formation of Arabidopsis Cryptochrome 2 photobodies in mammalian nuclei: Application as an optogenetic DNA damage checkpoint switch. *J. Biol. Chem.* **288**, 23244–23251 (2013). doi: 10.1074/jbc.M113.493361; pmid: 23833191
46. X. Yu *et al*., Formation of nuclear bodies of Arabidopsis CRY2 in response to blue light is associated with its blue light-dependent degradation. *Plant Cell* **21**, 118–130 (2009). doi: 10.1105/tpc.108.061663; pmid: 19141709
47. M.-T. Wei *et al*., Phase behaviour of disordered proteins underlying low density and high permeability of liquid organelles. *Nat. Chem.* **9**, 1118–1125 (2017). doi: 10.1038/nchem.2803; pmid: 29064502
48. H. I. Suzuki, R. A. Young, P. A. Sharp, Super-Enhancer-Mediated RNA Processing Revealed by Integrative MicroRNA Network Analysis. *Cell* **168**, 1000–1014.e15 (2017). doi: 10.1016/j.cell.2017.02.015; pmid: 28283057
49. J. E. Bradner, D. Hnisz, R. A. Young, Transcriptional Addiction in Cancer. *Cell* **168**, 629–643 (2017). doi: 10.1016/j.cell.2016.12.013; pmid: 28187285
50. M. Ptashne, How eukaryotic transcriptional activators work. *Nature* **335**, 683–689 (1988). doi: 10.1038/335683a0; pmid: 3050531
51. P. J. Mitchell, R. Tjian, Transcriptional regulation in mammalian cells by sequence-specific DNA binding proteins. *Science* **245**, 371–378 (1989). doi: 10.1126/science.2667136; pmid: 2667136
52. J. Liu *et al*., Intrinsic disorder in transcription factors. *Biochemistry* **45**, 6873–6888 (2006). doi: 10.1021/bi0602718; pmid: 16734424
53. H. Xie *et al*., Functional anthology of intrinsic disorder. 1. Biological processes and functions of proteins with long disordered regions. *J. Proteome Res.* **6**, 1882–1898 (2007). doi: 10.1021/pr060392u; pmid: 17391014
54. S. F. Banani *et al*., Compositional Control of Phase-Separated Cellular Bodies. *Cell* **166**, 651–663 (2016). doi: 10.1016/j.cell.2016.06.010; pmid: 27374333
55. R. A. Beagrie *et al*., Complex multi-enhancer contacts captured by genome architecture mapping. *Nature* **543**, 519–524 (2017). pmid: 28273065
56. S. S. P. Rao *et al*., Cohesin Loss Eliminates All Loop Domains. *Cell* **171**, 305–320.e24 (2017). doi: 10.1016/j.cell.2017.09.026; pmid: 28985562
57. W.-K. Cho *et al*., Mediator and RNA polymerase II clusters associate in transcription-dependent condensates. *Science* **361**, 412–415 (2018).
58. W.-K. Cho *et al*., RNA Polymerase II cluster dynamics predict mRNA output in living cells. *eLife* **5**, 1123 (2016). doi: 10.7554/eLife.13617; pmid: 27138339
59. A. G. Larson *et al*., Liquid droplet formation by HP1α suggests a role for phase separation in heterochromatin. *Nature* **547**, 236–240 (2017). doi: 10.1038/nature22822; pmid: 28636604
60. A. R. Strom *et al*., Phase separation drives heterochromatin domain formation. *Nature* **547**, 241–245 (2017). doi: 10.1038/nature22989; pmid: 28636597
61. M. Feric *et al*., Coexisting Liquid Phases Underlie Nucleolar Subcompartments. *Cell* **165**, 1686–1697 (2016). doi: 10.1016/j.cell.2016.04.047; pmid: 27212236
62. T. S. Harmon, A. S. Holehouse, M. K. Rosen, R. V. Pappu, Intrinsically disordered linkers determine the interplay between phase separation and gelation in multivalent proteins. *eLife* **6**, e30294 (2017). doi: 10.7554/eLife.30294; pmid: 29091028
63. J. A. Riback *et al*., Stress-Triggered Phase Separation Is an Adaptive, Evolutionarily Tuned Response. *Cell* **168**, 1028–1040.e19 (2017). doi: 10.1016/j.cell.2017.02.027; pmid: 28283059
64. S. Boeynaems *et al*., Phase Separation of C9orf72 Dipeptide Repeats Perturbs Stress Granule Dynamics. *Mol. Cell* **65**, 1044–1055.e5 (2017). doi: 10.1016/j.molcel.2017.02.013; pmid: 28306503
65. J. P. Brady *et al*., Structural and hydrodynamic properties of an intrinsically disordered region of a germ cell-specific protein on phase separation. *Proc. Natl. Acad. Sci. U.S.A.* **114**, E8194–E8203 (2017). doi: 10.1073/pnas.1706197114; pmid: 28894006
66. A. Patel *et al*., A Liquid-to-Solid Phase Transition of the ALS Protein FUS Accelerated by Disease Mutation. *Cell* **162**, 1066–1077 (2015). doi: 10.1016/j.cell.2015.07.047; pmid: 26317470
67. A. Molliex *et al*., Phase separation by low complexity domains promotes stress granule assembly and drives pathological fibrillization. *Cell* **163**, 123–133 (2015). doi: 10.1016/j.cell.2015.09.015; pmid: 26406374
68. A. Jain, R. D. Vale, RNA phase transitions in repeat expansion disorders. *Nature* **546**, 243–247 (2017). pmid: 28562589

ACKNOWLEDGMENTS

We thank W. Salmon of the W. M. Keck Microscopy Facility; D. Richardson and S. Terclavers of the Harvard Center for Biological Imaging; and T. Volkert, D. Reynolds, S. Mraz, and S. Gupta of the Whitehead Genome Technologies Core for technical

assistance. We thank the Imaging Platform at the Broad Institute for assistance with CellProfiler. **Funding:** The work was supported by NIH grants GM123511 (R.A.Y.) and P01-CA042063 (P.A.S.), NSF grant PHY-1743900 (A.K.C., R.A.Y., and P.A.S.), Koch Institute Support (core) grant P30-CA14051 from the NCI (P.A.S.), Damon Runyon Cancer Research Foundation Fellowship 2309-17 (B.R.S.), Swedish Research Council Postdoctoral Fellowship VR 2017-00372 (A.B.), a Hope Funds for Cancer Research fellowship (B.J.A.), an NSF Graduate Research Fellowship (A.V.Z.), a Cancer Research Institute Irvington Fellowship (Y.E.G.), American Cancer Society New England Division Postdoctoral Fellowship PF-16-146-01-DMC (D.S.D.), and a NWO Rubicon Fellowship (J.S.). **Author contributions:** B.R.S., A.D., and R.A.Y. conceptualized and organized the project and wrote the manuscript. A.D., A.B., J.C.M., and Y.E.G. performed cell-imaging experiments and image analysis. I.A.K. and A.V.Z. generated endogenously tagged cell lines. B.R.S. and A.B. performed ChIP-seq. B.R.S. and E.L.C. performed in vitro droplet assays and optoIDR experiments. K.S. and B.J.A. developed and performed image analysis and produced visualizations. B.J.A. performed ChIP-seq analysis and produced visualizations. N.M.H. produced and purified recombinant proteins. A.V.Z. helped with biochemical experiments. C.H.L. performed protein amino acid analysis. D.S.D. performed ChIA-PET analysis and visualization. B.R.S., I.A.K., E.L.C., J.S., and A.V.Z. generated constructs. S.M. performed in vitro transcription assays. D.H., E.V., T.I.L., I.I.C., R.G.R., P.A.S., A.K.C., and R.A.Y. provided input into experimental design and interpretation. P.A.S., A.K.C., and R.A.Y. acquired funding for this study. R.A.Y. supervised the project with help from T.I.L. and A.K.C. All authors contributed to editing the manuscript. **Competing interests:** The Whitehead Institute filed a patent application based on this paper. R.A.Y. is a founder and shareholder of Syros Pharmaceuticals, Camp4 Therapeutics, and Omega Therapeutics. B.J.A. and T.I.L. are shareholders of Syros Pharmaceuticals, and T.I.L. is a consultant to Camp4 Therapeutics. All other authors declare no competing interests. **Data and materials availability:** Datasets generated in this study have been deposited in the Gene Expression Omnibus under accession number GSE112808.

SUPPLEMENTARY MATERIALS

www.sciencemag.org/content/361/6400/eaar3958/suppl/DC1
Materials and Methods
Figs. S1 to S10
Tables S1 to S3
References (*69*–*82*)
Data S1

4 November 2017; resubmitted 9 April 2018
Accepted 6 June 2018
Published online 21 June 2018
10.1126/science.aar3958

Science

Coactivator condensation at super-enhancers links phase separation and gene control

Benjamin R. Sabari, Alessandra Dall'Agnese, Ann Boija, Isaac A. Klein, Eliot L. Coffey, Krishna Shrinivas, Brian J. Abraham, Nancy M. Hannett, Alicia V. Zamudio, John C. Manteiga, Charles H. Li, Yang E. Guo, Daniel S. Day, Jurian Schuijers, Eliza Vasile, Sohail Malik, Denes Hnisz, Tong Ihn Lee, Ibrahim I. Cisse, Robert G. Roeder, Phillip A. Sharp, Arup K. Chakraborty and Richard A. Young

Science **361** (6400), eaar3958.
DOI: 10.1126/science.aar3958originally published online June 21, 2018

Phase separation and gene control

Many components of eukaryotic transcription machinery—such as transcription factors and cofactors including BRD4, subunits of the Mediator complex, and RNA polymerase II—contain intrinsically disordered low-complexity domains. Now a conceptual framework connecting the nature and behavior of their interactions to their functions in transcription regulation is emerging (see the Perspective by Plys and Kingston). Chong *et al.* found that low-complexity domains of transcription factors form concentrated hubs via functionally relevant dynamic, multivalent, and sequence-specific protein-protein interaction. These hubs have the potential to phase-separate at higher concentrations. Indeed, Sabari *et al.* showed that at super-enhancers, BRD4 and Mediator form liquid-like condensates that compartmentalize and concentrate the transcription apparatus to maintain expression of key cell-identity genes. Cho *et al.* further revealed the differential sensitivity of Mediator and RNA polymerase II condensates to selective transcription inhibitors and how their dynamic interactions might initiate transcription elongation.

Science, this issue p. eaar2555, p. eaar3958, p. 412; see also p. 329